Nuclear Materials and Energy 46 (2026) 102077

Contents lists available at ScienceDirect

Nuclear Materials and Energy

journal homepage: www.elsevier.com/locate/nme

Improved material mixing model in ERO2.0: Nonlinear effect of boron concentration on tungsten sputtering and influx from mixed tungsten-boron surfaces☆

H.A. Kumpulainen [a,*], S. Brezinsek [a], J. Romazanov [a], A. Kirschner [a], C. Baumann [a], K. Schmid [b], JET contributors[1]

[a] Forschungszentrum Jülich GmbH, Jülich, Germany
[b] Max–Planck-Institut für Plasmaphysik, Garching, Germany

ARTICLE INFO

Keywords:
Tungsten
Boron
Sputtering
Mixed materials
SDTrimSP
ERO2.0

ABSTRACT

An upgraded homogeneous mixing model for plasma-facing surfaces in ERO2.0 has been developed using a database of SDTrimSP mixed-material simulations, replacing earlier linear interpolation between pure-material sputtering yields. The SDTrimSP simulations predict nonlinear relationships between tungsten sputtering yield and low-Z surface concentration, in particular increased tungsten erosion by deuterium from tungsten-boron surfaces at low impact energies (<300 eV). The updated model features parameterised analytic fit formulas for the sputtered energy and angular distributions, offering higher sampling resolution, significantly reduced memory requirements, and improved robustness against Monte Carlo noise compared to tabulated SDTrimSP outputs. As the first application of the model in an inter-ELM H-mode JET plasma scenario, ERO2.0 simulations predict that introducing a 10% B surface concentration on W divertor components reduces total W erosion by 7%, primarily due to B ions, but increases W erosion and influx from D atom impact by 5% at the outer divertor entrance.

1. Introduction

Understanding the performance of plasma-facing components (PFCs) is essential for the development and efficient operation of magnetic confinement fusion devices. Tungsten (W) is the plasma-facing material selected for ITER [1] and DEMO [2] due to its low tritium retention and high resilience to sputtering and heat loads. However, W impurities in the core plasma strongly degrade energy confinement via W radiation [3]. Thus, achieving optimal plasma performance requires the ability to identify and mitigate W sources in any wall regions which lack sufficient W screening.

In accordance with the recent ITER baseline update to a W first wall [1], boronization is the foreseen wall conditioning method to getter oxygen and reduce high-Z impurity sources in the absence of beryllium [4]. Accurately modelling the surface mixing of light elements such as boron (B) with W, and impurity transport from such mixed-material surfaces, is crucial for predicting impurity influx into the plasma and its impact on energy confinement due to radiative losses. In this context, the 3D Monte Carlo impurity transport and plasma-wall interaction code package ERO2.0 [5] is developed to simulate material erosion, deposition, and impurity transport in edge plasmas.

This work presents an upgraded material mixing model implemented in ERO2.0 that incorporates the nonlinear dependence of sputtering yields on the local material concentrations. The former implementation of material mixing in ERO2.0 involves a linear interpolation of sputtering yields calculated for pure materials, now replaced with a dedicated SDTrimSP simulation database for mixed-material targets. The initial energy and angular distributions calculated by SDTrimSP are characterised by introducing parametric regression functions. The new ERO2.0 features are verified in a simulation study on the impact of boron surface concentration on W gross and net erosion and influx from the JET W divertor, based on an inter-ELM H-mode plasma scenario with experimentally validated plasma profiles.

2. SDTrimSP simulations of mixed-material sputtering

The sputtering and reflection calculations in ERO2.0 make use of pre-computed databases compiled from SDTrimSP [6] binary-collision

☆ This article is part of a Special issue entitled: 'PFMC-20' published in Nuclear Materials and Energy.

* Corresponding author.
E-mail address: h.kumpulainen@fz-juelich.de (H.A. Kumpulainen).

[1] See the author list of "Overview of T and D-T results in JET with ITER-like wall" by CF Maggi et al. 2024 Nucl. Fusion 64 112012.

https://doi.org/10.1016/j.nme.2026.102077
Received 16 July 2025; Received in revised form 31 October 2025; Accepted 28 January 2026
Available online 29 January 2026

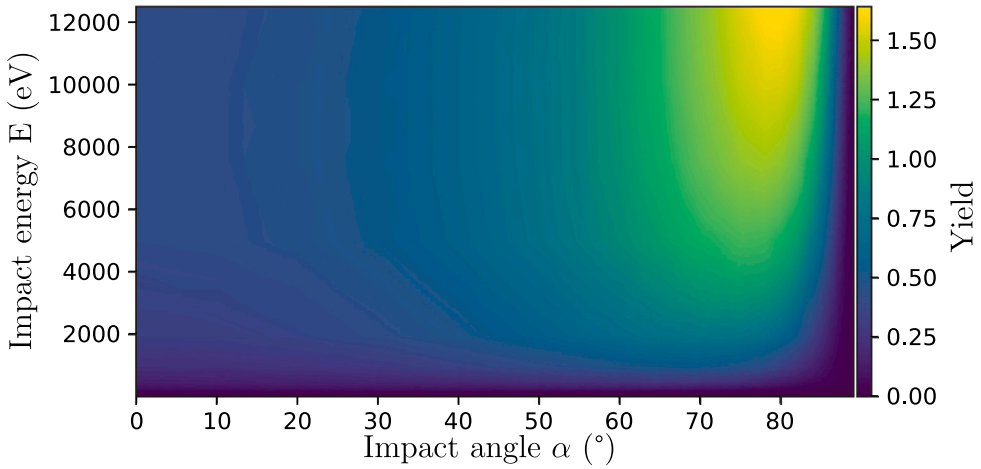

Fig. 1. Sputtering yield of W from a W90 B10 mixed surface due to B projectiles as a function of impact energy and angle, calculated using SDTrimSP.

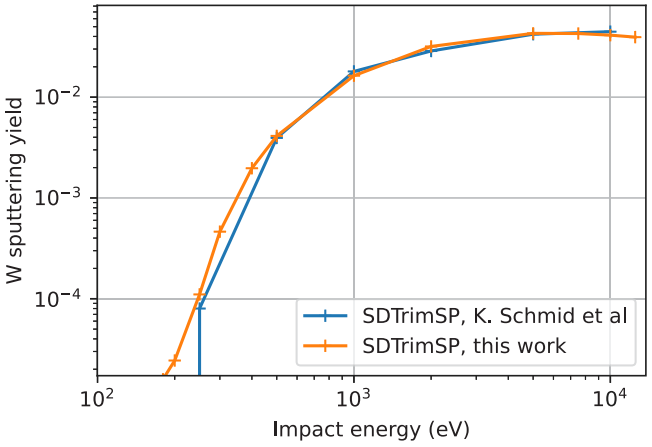

Fig. 2. Benchmark of earlier [8] and new SDTrimSP simulations of W sputtering from a W90 Be10 mixed surface by D projectiles at an impact angle of 65° as a function of the impact energy.

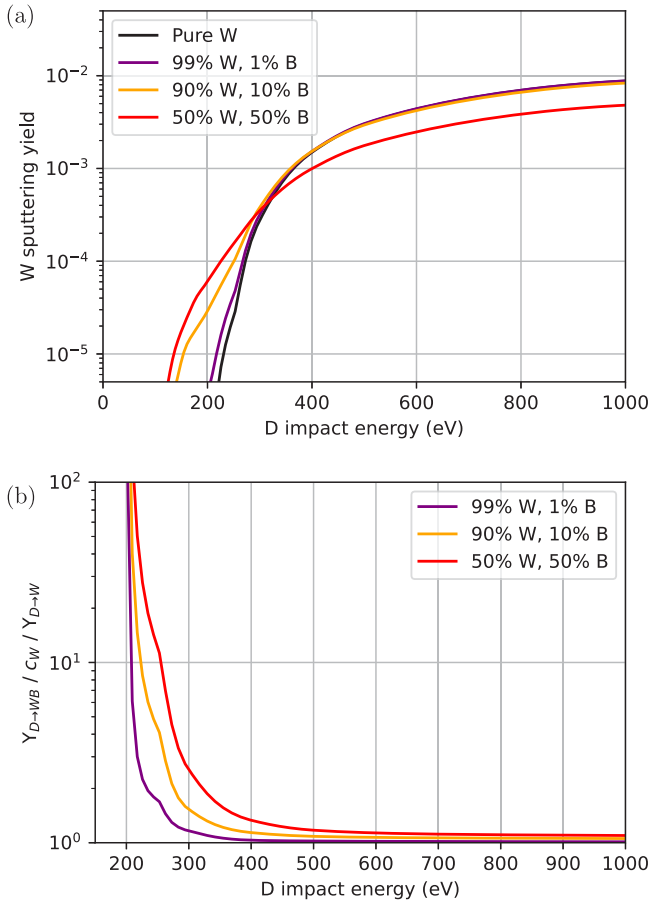

Fig. 3. (a) Sputtering yield of W by D projectiles calculated by SDTrimSP as a function of impact energy at a constant impact angle of 60° for a pure W surface and mixed W-B surfaces with various B surface concentrations. (b) Ratio of W sputtering yields by D from mixed W-B surfaces relative to pure W, adjusted for W concentration such that a ratio of 1 indicates a linear relationship between W concentration and W yield.

Monte Carlo simulations. Prior to this work, ERO2.0 studies involving mixed-material surfaces applied a homogeneous material mixing model (HMM) [7] which linearly interpolates SDTrimSP sputtering yields calculated for pure materials. In this contribution, the HMM is extended to include the non-linear relationships between surface composition and sputtering yields by incorporating dedicated mixed-material SDTrimSP simulations in the ERO2.0 sputtering database.

The initial mixed-material sputtering database for ERO2.0 consists of the binary target material combinations W-B, W-Be, and W-D. The projectile species include H, D, T, He, Be, B, Ne, Ar, and W. The W surface concentration is scanned from 1% to 99%, the impact energy from 1 eV to 12500 eV, and the impact angle from 0° to 89° (Fig. 1). The target structure is assumed to be amorphous. The Krypton-Carbon (KrC) interatomic potential [9] is applied. The surface binding energy model for mixed materials is the weighted average of the pure-element surface binding energies. Due to concerns that the averaged surface binding energy is potentially a suboptimal approximation for targets with a high surface concentration of gases such as D, a lower bound of half the pure-W binding energy is being considered for revised simulations of sputtering from W-D surfaces [10].

The calculated W and Be sputtering yields from mixed W-Be surfaces were benchmarked against an established SDTrimSP dataset [8] created for the WALLDYN material migration code [11] (Fig. 2). The new SDTrimSP calculations were confirmed to be consistent with the previous results, with the added benefits of increased impact energy and angle resolution and reduced variance, particularly at low sputtering yields, due to increasing the followed trajectory count from 100 000 to 32 million per simulation.

Adding a higher B surface concentration to a W-B target causes a lower impact energy threshold for W sputtering by D projectiles and an

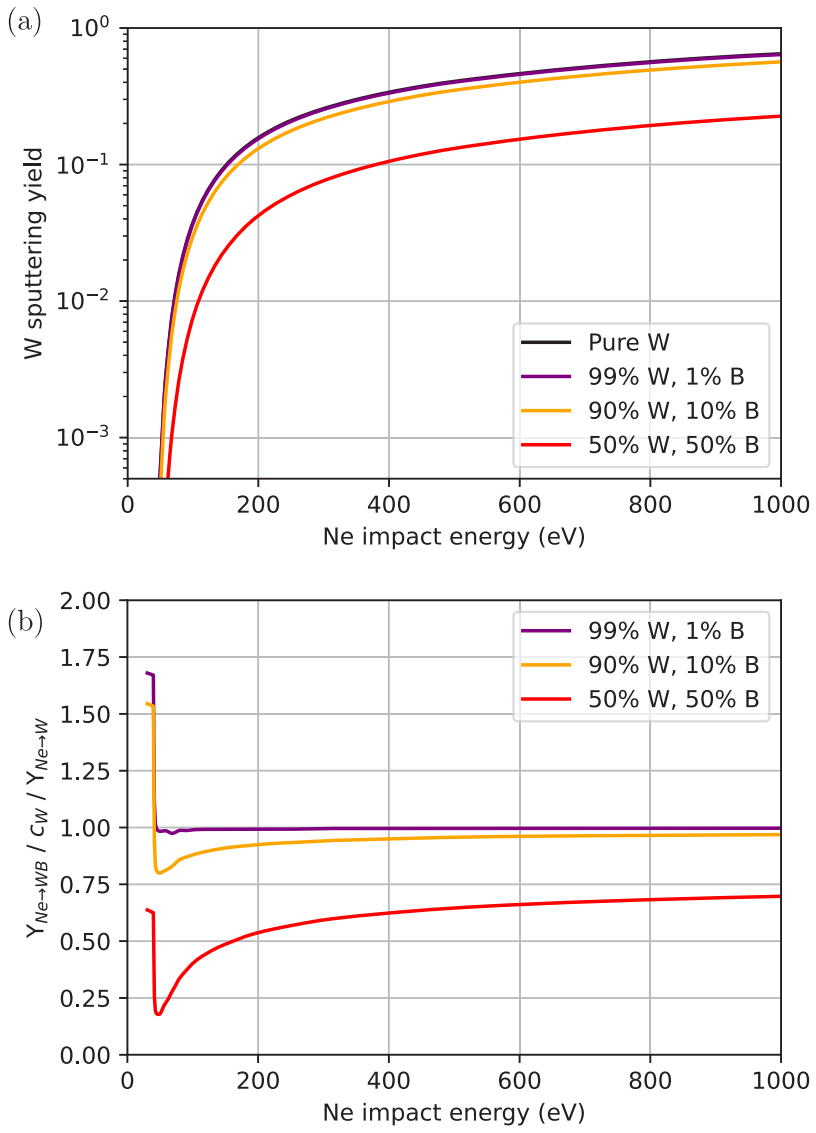

Fig. 4. (a) Sputtering yield of W by Ne projectiles calculated by SDTrimSP as a function of impact energy at a constant impact angle of 60° for a pure W surface and mixed W-B surfaces with various B surface concentrations. (b) Ratio of W sputtering yields by Ne from mixed W-B surfaces relative to pure W, adjusted for W concentration such that a ratio of 1 indicates a linear relationship between W concentration and W yield.

increased W sputtering yield at impact energies below 300 eV, whereas at energies above 400 eV the W yield decreases as a function of B surface concentration (Fig. 3a). Due to the B atoms having a higher mass (11 amu) than D (2 amu) but lower than W (184 amu), the energy of D projectiles is transferred to W atoms more efficiently when B is present. In the limit of high impact energy, dilution of the W surface concentration by B is the dominant effect, whereas near the sputtering threshold the ratio of mixed W-B to pure-W sputtering yields tends to infinity as the pure-W yield tends to zero (Fig. 3b).

In contrast to D projectiles, the W yield due to Ne projectiles (20 amu) is a decreasing function of the B surface concentration at impact energies greater than 45 eV (Fig. 4a). The reduction of the W yield with increasing B concentration is stronger than linear, indicating preferential low-Z sputtering and reduced energy transfer from Ne to W in the presence of B (Fig. 4b). Only at an impact energy of approximately 40 eV is the increase in W yield due to reduced surface binding energy significant enough to overcome the competing effects of reduced energy transfer and diluted W concentration.

3. Analytic fitted descriptions of the SDTrimSP sputtered distributions

In this section, the sputtered energy, polar angle, and azimuthal angle distributions from SDTrimSP are characterised using parameterised analytic functions (Eqs. (1)- (3)). A common approximation for the sputtered energy distribution is the Thompson distribution [12], which is generalised here (Eq. (1)) by allowing the energy exponent C_1, the maximum sputtered energy C_2, and the surface binding energy C_3 to vary as fitting parameters. The allowable parameter values are bounded such that all three parameters are non-negative, C_1 and C_3 cannot exceed 100, and C_2 cannot exceed the impact energy (all energies given in eV). While the maximum sputtered energy and the surface binding energy have a distinct physical interpretation in the original Thompson distribution, here the parameters are optimised to the values which produce the closest overall agreement with SDTrimSP data, even if those values differ from empirical expectations based on their interpretation. The parameterised energy distribution function closely

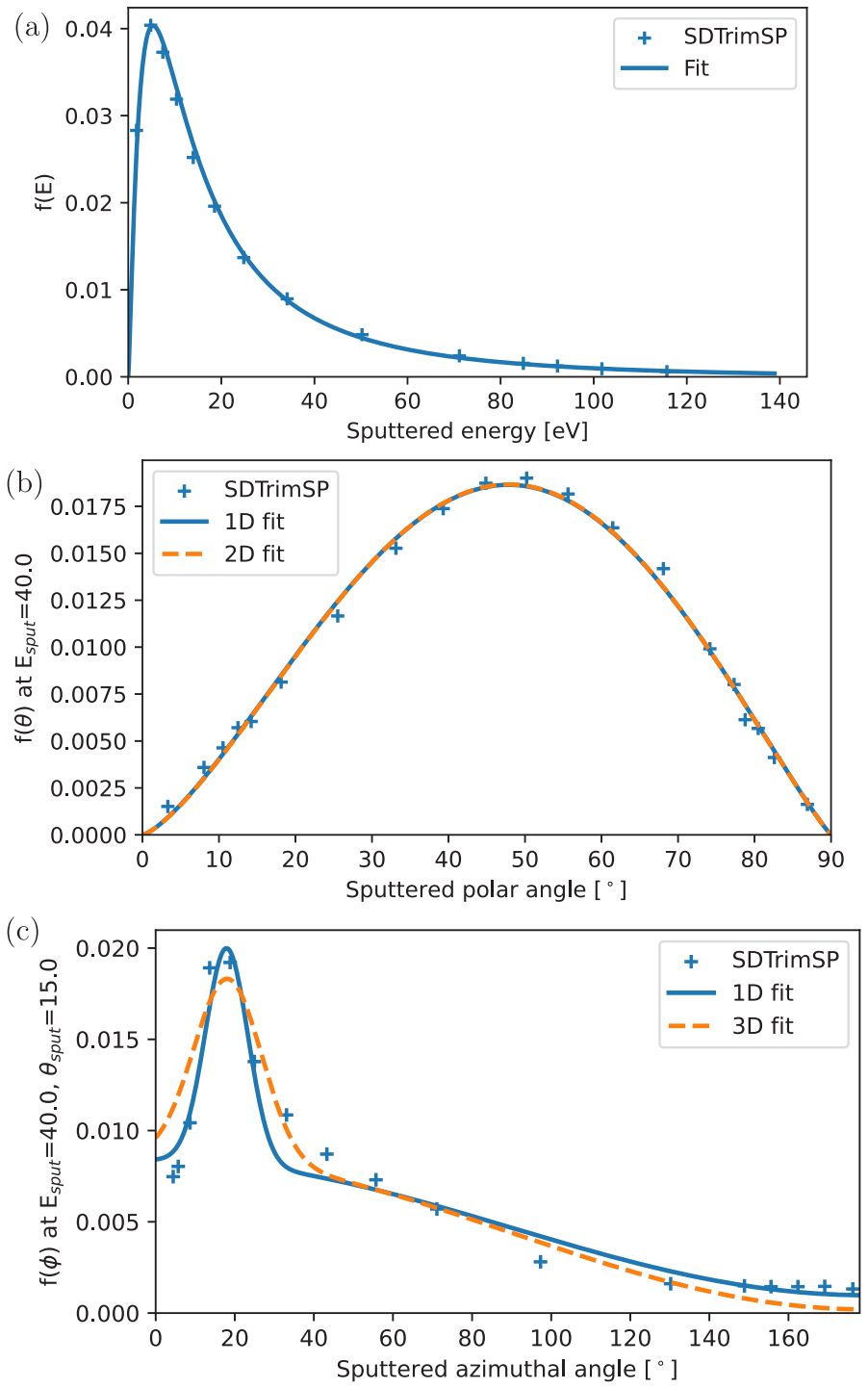

Fig. 5. Probability distributions for (a) energy, (b) polar angle at a constant sputtered energy E_{sput}, and (c) azimuthal angle at a constant E_{sput} and polar angle θ_{sput} of sputtered W atoms due to B impact (E_{impact} = 1 keV, α=60°) on a 90% W - 10% B mixed surface calculated using SDTrimSP (blue markers), univariate fits (blue solid lines), and multivariate energy-angular fits (orange dashed lines) based on Eqs. (1), (2), and (3).

reproduces the SDTrimSP calculation results and is more robust against Monte Carlo noise than nearest, linear, or spline interpolation of the tabulated SDTrimSP data (Fig. 5a).

$$f(E) = A_{norm}\, E^{C_1}\, \frac{1-\sqrt{E/C_2}}{(E+C_3)^{C_1+2}} \tag{1}$$

$$f(E,\theta) = A_{norm}\, f(E)\, \sin^{C_4}\theta\, \cos^{C_5}\theta \tag{2}$$

$$f(E,\theta,\phi) = A_{norm}\, f(E,\theta)\left(1 + C_6\cos\phi + C_7\exp\left(-\left(\frac{\phi - C_8}{C_9}\right)^2\right)\right) \tag{3}$$

The numerical method for optimising the energy and angular fit parameters is an iteratively converging least-squares logarithmic grid search. Starting from an initial value, the relative mean squared error (MSE) of the fit is evaluated within a discretised range of parameters. A

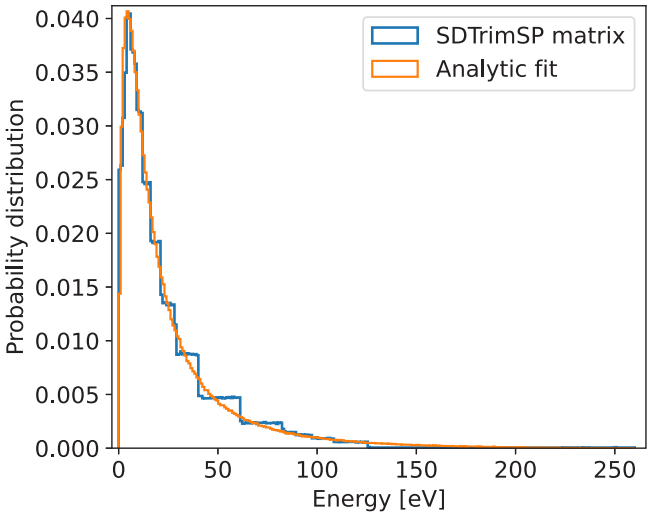

Fig. 6. Initial energy distribution of sputtered W sampled in an ERO2.0 simulation based on SDTrimSP matrix output (blue) and an analytic description fitted to the same SDTrimSP data (orange). Monoenergetic B projectiles with E_{impact} = 1 keV and a constant 60° incidence angle on a pure W target were assumed for this benchmark simulation.

logarithmic transform is applied to the parameter evaluation interval, meaning that the ratio between consecutive evaluated parameter values in each dimension is constant. The best-fit (lowest relative MSE) parameter combination is selected as the initial value for the next search iteration. The search converges by iteratively reducing the parameter space towards the vicinity of the current best-fit combination and thereby also refining the resolution of the grid search for subsequent iterations. Gradient descent methods were also explored, but rejected due to frequent trapping in local optima far from the global optimum.

The sputtered polar angle distribution is described as a product of sine and cosine raised to the power of fitted exponents C_4 for the sine and C_5 for the cosine (Eq. (2)). The optimised value of both exponents is generally close to 1 at low sputtered energies, but in many cases the distribution is skewed towards more normal or tangential sputtered angles within the high-energy tail of the sputtered energy distribution. For example, in the case of B projectiles on a W90 B10 mixed surface at 1 keV and 60° impact, the best-fit exponents at E_{sput} = 40 eV are $C_4 = 1.35$ and $C_5 = 1.11$ (Fig. 5b).

To avoid the need to tabulate the sputtered energies for the polar angle distribution functions, a bivariate (2D) energy-angular fit is introduced in addition to the univariate (1D) angular fit at a constant energy. In the 2D fit, the fit parameters C_4 and C_5 are not energy-independent constants but 5th degree polynomial functions of the sputtered energy. Under typical circumstances with low Monte Carlo noise in the tabulated distributions from SDTrimSP, the analytic fitted 1D and 2D polar angle distributions are nearly identical (Fig. 5b).

The azimuthal angle distribution is described as the sum of three terms: (i) an uniform component, dominant at normal incidence, (ii) a cosine component, dominant at shallow incidence and low sputtered energy, and (iii) a Gaussian component, frequently observed at shallow incidence and high sputtered energy (Eq. (3)). The fitted parameters represent the amplitude of the cosine C_6, the amplitude of the Gaussian C_7, the mean of the Gaussian (azimuthal location of the peak) C_8, and the standard deviation of the Gaussian (width of the peak) C_9 (Fig. 5c).

Similar to the 2D energy-angular distribution describing the dependence of the polar angle on the sputtered energy, a 3D energy-polar-azimuthal distribution function is introduced to describe the complete sputtered distribution function (Fig. 5c). In the 3D fit, the azimuthal fit parameters C_6 to C_9 are 5th degree polynomial functions of the sputtered polar angle, and each of the polynomial coefficients is represented as a 5th degree polynomial fit with respect to the sputtered energy. After optimising the parameter values, the sputtered energy, polar angle, and azimuthal angle distribution functions are scaled by a normalisation factor A_{norm} such that the total probability is 1. Storing the fitted parameters for each combination of one projectile species and two sputtered target material components, including parameter scans over material concentration, impact energy, and impact angle, requires 12 to 18 MB of storage space, compared to 1300 MB for the tabulated SDTrimSP format.

During the 3D fit parameter optimisation process, the parameters for sputtered energies are determined first, then the sputtered polar angles, and last the azimuthal angles which are the least important for ERO2.0 simulations. Thus, the 1D and 3D fits for the sputtered energy are equal, whereas the 3D fit for azimuthal angles is affected by compounding fit residuals from the energies and polar angles, making it on average less accurate than the 1D azimuthal fit. The SDTrimSP angular distributions are also affected by higher statistical noise than the sputtered energy because the sputtered energy distribution used for fitting is integrated over the angles but not vice versa.

The analytic descriptions of the sputtered distributions implemented in ERO2.0 were benchmarked against the earlier approach of a tabulated cumulative distribution function (CDF), demonstrating an improved resolution for the sputtered energy distribution (Fig. 6). The ERO2.0 inverse transform sampling method for sputtered energies uses linear interpolation for tabulated CDFs, resulting in piecewise constant energy distributions if the CDF values are tabulated but smooth energy distributions if the CDF is described as an infinitely differentiable analytic function (at $E > 0$).

Furthermore, the sampling of sputtered energies is greatly improved in the energy range between the highest energy value listed in the tabulated format ($E_{sput} > 126$ eV in Fig. 6) and the highest physically justified energy. Sampling the analytic fits yields 5 to 8 times more sputtered atoms in the sputtered energy range 126 to 150 eV than sampling from the tabulated CDF (analytic fit probability 3 to $5 \cdot 10^{-4}$/eV, tabulated $6{\cdot}10^{-5}$/eV). The sputtered atoms with the highest energy have the longest ionisation mean-free path and thus the highest probability of avoiding local redeposition, which makes accurate energy sampling exceptionally important for the high-energy tail of the distribution.

4. ERO2.0 simulations of mixed-material sputtering in JET

The impact of the nonlinear mixed-material sputtering yields and the parametric sputtered distributions on the W erosion and influx is studied by ERO2.0 simulations of a JET H-mode inter-ELM plasma scenario validated in previous studies [13,14]. The scenario has a toroidal axial magnetic field of 2.5 T, a plasma current of 2.3 MA, and heating 15 MW from neutral beam injection + 3 MW from ion cyclotron resonance heating. The electron density at the outer divertor target is of order 10^{20} m^{-3} and the electron temperature approximately 40 eV. The background plasma conditions are based on simulations using the EDGE2D-EIRENE code [15] and validated against upstream and divertor measurements. Following the ITER decision to replace Be with W as a first wall material [1], this work focuses on W-B rather than W-Be mixing by imposing B instead of Be as the main low-Z impurity with a constant concentration of 0.5% in the plasma. Two simulations with different surface assumptions are compared: a pure W divertor without any deposit layers, and a constant 10% B surface concentration on all divertor components.

The primary cause of the predicted gross and net W erosion is B ion impact at the outer and inner divertor targets (tiles 5 and 3 respectively) and on tile 1 in the high-field side far SOL (Fig. 7a). The contribution of D ions is negligible due to low electron temperature, and the contribution of W self-sputtering is only a few percent of the total W erosion. The low self-sputtering is due to effective W screening

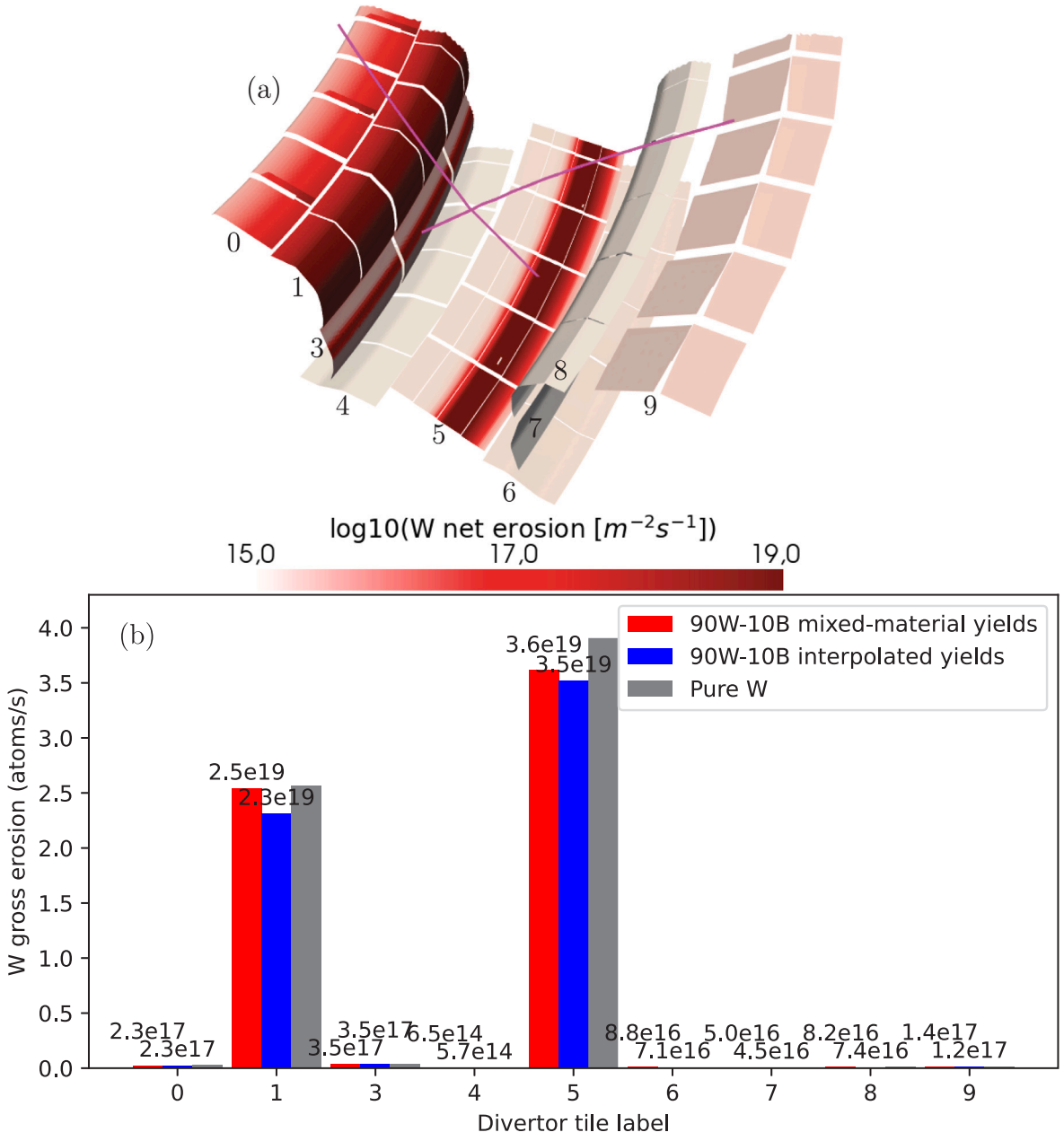

Fig. 7. (a) Net erosion rate of W in the JET divertor predicted by ERO2.0 during the inter-ELM phase of discharge #94606 at 10 s, assuming a pure W divertor without any deposit layers or surface mixing. The divertor tiles 0 to 9 are labelled. (b) Gross erosion rate of W integrated over the area of each divertor tile, calculated using the upgraded (mixed-material yields, red) and earlier (interpolated yields, blue) material mixing model with a 90% W and 10% B surface, and compared against a pure W surface (grey). The erosion rates for mixed-material and interpolated yields are also displayed as numbers.

on tiles 1, 3, and 5 by prompt redeposition, SOL flows, and electric fields, leading to short dwell times in the plasma and preventing W ionisation to high charge states.

The predicted net effect of imposing a 10% B surface concentration in the JET divertor is a 7% reduction in the total W erosion rate. The mixed-material yields result in 4% higher total W erosion, varying from −1% to 24% by divertor tile, than the previous material mixing implementation with linearly interpolated pure-element sputtering yields (Fig. 7b). In regions with low incident ion flux and maximum B impact energies barely above the sputtering threshold, the (negligible) W erosion rate increases with B surface concentration due to the reduced surface binding energy of W-B.

The predicted high W erosion rate (> 10^{18}/m^2/s) on tile 1 (Fig. 7a) occurs due to the assumed absence of any deposit layers and does not represent a steady state. In JET experiments [16] and earlier simulations based on the Be-W wall [13,14], beryllium-rich deposit layers covering tiles 0 and 1 suppress most of the net erosion of W due to impurity ion impact on the high-field side divertor shoulder. The hypothetical 100% and 90% W surface concentrations in the presented simulations are imposed for comparison purposes only.

Considering that the W content in the core plasma predicted by ERO2.0 in the studied plasma scenario is not caused by W erosion by ions at the divertor targets, but almost entirely due to sputtering by D atoms from tiles 8 and 9 near the outer divertor entrance [14],

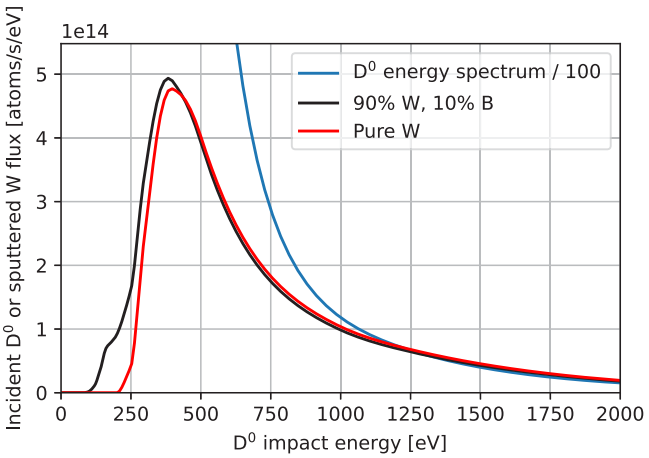

Fig. 8. Erosion rate of W due to D atom impact in the JET outer vertical divertor (tiles 7, 8, and 9) at each D impact energy, assuming a pure W divertor (red) or a constant 10% surface concentration of B (black) based on W yields from SDTrimSP and D fluxes from EIRENE. The energy spectrum of incident D atoms (divided by 100) is shown in blue.

special attention is paid to modelling the D^0 flux and energy-angular impact spectrum [17] using EIRENE [18] simulations (Fig. 8). The W erosion rate is obtained as a function of impact energy by multiplying the SDTrimSP sputtering yields by the bivariate D^0 impact distribution and integrating over the impact angles. While the W sputtering yield in the case of a 10% B concentration is significantly higher than for pure W at E_{impact} <300 eV, the vast majority of W sputtering occurs at E_{impact} >300 eV. The net effect of introducing B is thus only a 5% increase in the W sputtering rate by D^0 and W influx from the outer divertor entrance.

5. Conclusions

The homogeneous mixing model for plasma-facing surfaces in ERO2.0 has been upgraded with a new database of dedicated SDTrimSP mixed-material simulations, replacing the earlier linear interpolation of pure-material sputtering yields. The sputtered energy and angular distributions in the new database are described as parameterised analytic multivariate functions, which provide higher sampling resolution, two orders of magnitude lower memory and storage needs, and higher resilience to Monte Carlo noise than the previous approach of tabulated SDTrimSP output.

The first application and benchmark of the updated mixing model in ERO2.0 simulations leverages an experimentally validated inter-ELM H-mode JET plasma scenario to compare the W erosion rates between a hypothetical pure W divertor and an imposed B surface concentration of 10% on all divertor components, considering the gross and net erosion of W due to impurities, fuel ions, and atoms. ERO2.0 predicts that the net impact of imposing the 10% B surface concentration is a 7% reduction in total W erosion at the divertor targets, mainly due to B ions, but a 5% increase in W erosion and influx due to D atom impact at the outer divertor entrance.

Validating the mixed-material SDTrimSP calculations with experiments would strengthen confidence in their predictive accuracy. Additional prospects for further improving the database include the modelling of surface roughness effects and material combinations consisting of more than two elements.

CRediT authorship contribution statement

H.A. Kumpulainen: Writing – review & editing, Writing – original draft, Visualization, Validation, Software, Methodology, Investigation, Funding acquisition, Formal analysis, Data curation, Conceptualization. **S. Brezinsek:** Writing – review & editing, Supervision, Project administration, Funding acquisition. **J. Romazanov:** Writing – review & editing, Visualization, Software, Methodology. **A. Kirschner:** Writing – review & editing, Supervision, Methodology. **C. Baumann:** Writing – review & editing, Validation, Software, Data curation. **K. Schmid:** Writing – review & editing, Validation, Software, Methodology, Data curation.

Declaration of competing interest

The authors declare that they have no known competing financial interests or personal relationships that could have appeared to influence the work reported in this paper.

Acknowledgements

This work is financially supported by a research grant awarded by the Finnish Cultural Foundation.

This work has been carried out within the framework of the EUROfusion Consortium, funded by the European Union via the Euratom Research and Training Programme (Grant Agreement No 101052200 — EUROfusion). Views and opinions expressed are however those of the author(s) only and do not necessarily reflect those of the European Union or the European Commission. Neither the European Union nor the European Commission can be held responsible for them.

The authors gratefully acknowledge computing time on the supercomputer JURECA [19] at Forschungszentrum Jülich under Grant No. CJIEK43.

Data availability

Data will be made available on request.

References

[1] P. Barabaschi, et al., Fus. Eng. Des. 215 (2025) 114990.
[2] T.R. Barrett, et al., Fus. Eng. Des. 109–111 (2016) 917–924.
[3] T. Pütterich, et al., Nucl. Fusion 50 (2010) 025012.
[4] T. Wauters, et al., Nucl. Mater. Energy 42 (2025) 101891.
[5] J. Romazanov, et al., Nucl. Mater. Energy 18 (2019) 331–338.
[6] A. Mutzke, et al., 2019 SDTrimSP version 6.00 IPP-report, 2019.
[7] M. Navarro, et al., 2021 63rd Annual Meeting of the APS DPP, Pittsburgh, 2021, O08.00007 https://meetings.aps.org/Meeting/DPP21/Content/4081.
[8] K. Schmid, et al., J. Nucl. Mater. 463 (2015) 66–72.
[9] W.D. Wilson, et al., Phys. Rev. B 15 (1977) 2458.
[10] U. von Toussaint, 2025, Private communication.
[11] K. Schmid, et al., J. Nucl. Mater. 415 (2011) S284–S288.
[12] M.W. Thompson, et al., Phil. Mag. 18 (1968) 377.
[13] H.A. Kumpulainen, et al., Nucl. Mater. Energy 33 (2022) 101264.
[14] H.A. Kumpulainen, et al., Plasma Phys. Control. Fusion 66 (2024) 055007.
[15] R. Simonini, et al., Contrib. Plasma Phys. 34 (1994) 368–373.
[16] A. Widdowson, et al., Nucl. Mater. Energy 19 (2019) 218–224.
[17] H.A. Kumpulainen, et al., Plasma Phys. Control. Fusion 67 (2025) 055044.
[18] D. Reiter, et al., Fusion Sci. Technol. 47 (2005) 172.
[19] P. Thörnig, J. Large-Scale Res. Facil. 7 (2021) A182.